J Mater Sci (2009) 44:2046–2054
DOI 10.1007/s10853-009-3283-4

Microstructure, tensile properties, and creep behavior of high-pressure die-cast Mg–4Al–4RE–0.4Mn (RE = La, Ce) alloys

Jinghuai Zhang · Ke Liu · Daqing Fang · Xin Qiu · Dingxiang Tang · Jian Meng

Received: 7 August 2008 / Accepted: 20 January 2009 / Published online: 26 February 2009

Abstract High-pressure die-cast (HPDC) Mg–4Al–4RE–0.4Mn (RE = La, Ce) magnesium alloys were prepared and their microstructures, tensile properties, and creep behavior have been investigated in detail. The results show that two binary Al–Ce phases, $Al_{11}Ce_3$ and Al_2Ce, are formed mainly along grain boundaries in Mg–4Al–4Ce–0.4Mn alloy, while the phase composition of Mg–4Al–4La–0.4Mn alloy contains only α-Mg and $Al_{11}La_3$. The $Al_{11}La_3$ phase comprises large coverage of the grain boundary region and complicated morphologies. Compared with $Al_{11}Ce_3$ phase, the higher volume fraction and better thermal stability of $Al_{11}La_3$ have resulted in better-fortified grain boundaries of the Mg–4Al–4La–0.4Mn alloy. Thus higher tensile strength and creep resistance could be obtained in Mg–4Al–4La–0.4Mn alloy in comparison with that of Mg–4Al–4Ce–0.4Mn. Results of the theoretical calculation that the stability of $Al_{11}La_3$ is the highest among four Al–RE intermetallic compounds supports the experimental results further.

Introduction

As the lightest of metallic structural materials, magnesium alloy die-castings are very suitable for automotive applications because vehicle weight reduction and consequently energy saving are becoming the world focus. Some commercial high-pressure die-cast (HPDC) Mg–Al alloys, for instance, AZ91D, AM60B, and AM50A, owing to their excellent castability and acceptable room temperature mechanical properties, have already been successfully introduced into certain automobile parts such as instrument panels, seat frames, and steering wheels. However, due to their poor elevated temperature mechanical properties none of these alloys can be applied to power train parts operating at temperatures higher than 120 °C [1–3].

Accordingly, enormous efforts have been made to explore heat-resistant HPDC magnesium alloys and several alloy systems have been developed, such as Mg–Al–RE (RE = rare earth), Mg–Al–Si, and Mg–Al–Ca/Sr alloys [1–8]. One of such alloys to be developed was AE42 (Mg–4Al–2RE) which contained relatively thermally stable $Al_{11}RE_3$ precipitates and the complete suppression of $Mg_{17}Al_{12}$ phase [1]. Unfortunately, the decomposition of $Al_{11}RE_3$ phase resulting in deteriorated creep resistance at temperatures above 150 °C has been reported [9].

Recently, a new HPDC alloy developed by Hydro Magnesium [10], AE44, which has more attractive high temperature mechanical properties than AE42 alloy, has been successfully used for producing large structural magnesium castings. However, the REs used in AE42 and AE44 are Ce-rich misch metal (typical composition is 52–55 wt% Ce, 23–25 wt% La, 16–20 wt% Nd, and 5–6 wt% Pr) [9]. As a result, even for AE44, the decline of its creep properties at high temperature has not been resolved completely (this conclusion was also obtained from our own experimental results). Since the presence of Al–RE phases plays a significant role in affecting the mechanical properties of Mg–Al–RE (AE) series of HPDC alloys, its further investigation is necessary and useful for future alloy design. Herein, single RE element, Ce or La, AE alloys

J. Zhang · K. Liu · D. Fang · X. Qiu · D. Tang · J. Meng (✉)
State Key Laboratory of Rare Earth Resources Application, Changchun Institute of Applied Chemistry, Chinese Academy of Sciences, Changchun 130022, China
e-mail: jmeng@ciac.jl.cn

J. Zhang · K. Liu
Graduate School of the Chinese Academy of Science, Beijing 100049, China
e-mail: zjhhhxx@ciac.jl.cn

were prepared to explore the influences of Al–RE phases on the microstructures and mechanical properties of the AE alloys.

Experimental procedure

The nominal compositions of the experimental alloys were Mg–4Al–4Ce–0.4Mn and Mg–4Al–4La–0.4Mn, respectively. Commercial pure Mg and Al were used and Mn, La, and Ce were added as Al–10 wt% Mn, Mg–20 wt% La, and Mg–20 wt% Ce master alloys, respectively. The chemical compositions of the alloys were determined by inductively coupled plasma atomic emission spectroscopy (ICP-AES) and the results are listed in Table 1. Hereafter, the marks given in Table 1, which indicate alloy compositions, are used as alloy names.

Specimens were HPDC using a 280 ton-clamping force, cold chamber die-casting machine. The properties of the alloys referred to in this article were obtained on the separate die-cast test bars. Figure 1 shows the complete casting from the test bar die. The tensile test bar was 75 mm in gauge length and 6.1 mm in gauge diameter and the reported value was averaged over five measurements. The tensile creep tests were carried out on the specimens of cylindrical geometry with a 100 mm gauge length and 10 mm diameter cross-section.

Table 1 Chemical compositions of the investigated alloys (wt%)

Alloy	Al	RE	Mn	Mg
AlCe44	3.62	3.83	0.43	Balance
AlLa44	3.71	3.94	0.47	Balance

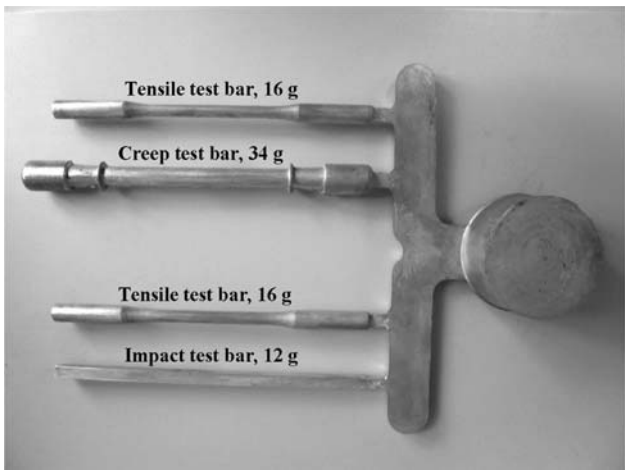

Fig. 1 Complete casting from the test bar die

Metallographic samples were cut from the same segments of the tensile or creep bars. To reveal the microstructures, the specimen surfaces were etched with 4% nitric acid solution and observed by scanning electron microscope (SEM) equipped with an energy dispersive X-ray spectrometer (EDS). The average grain size of the alloys was measured by linear intercept method and the analytical system of metallographic image (OLYCIA m3) was used to measure the volume fraction of secondary phases. The phase identification was confirmed by X-ray diffractometry (XRD).

Results and discussion

Analysis of microstructures

Figure 2a and b shows the cross-section microstructures of AlLa44 and AlCe44 alloys, respectively. Both typically comprise a skin region and an interior region. Further observation indicates that the skin could extend into the sample from 50 μm to more than 100 μm and its microstructure differs significantly from that observed in the interior. Much finer microstructures, whose grain/dendrite sizes are smaller than those in the interior, could be clearly observed in the skin region. It could be concluded that such a compact cast surface layer should have great benefits for the enhancement of the casting's strength [11]. Occasionally, a few large grains could be observed in the interior region, presumably originating as the large, isolated, and solid floating crystals in the melted metal flowing into the die cavity from the shot sleeve. Furthermore, we could also observe more shrinkage porosity in the interior region, which is mainly ascribed to the air trapped in the mold cavity. The air in the gas pores takes the role of a heat-insulating medium, which could retard heat transfer in the melt efficiently as compared with regions without porosity. Therefore, in such regions the local solidification rate is low and the structure with shrinkage porosity could form in the process of solidification [12]. Table 2 gives the average grain size and volume fraction of eutectic of the two alloys in skin and core regions, respectively. In HPDC AlLa44 alloy the average grain sizes from skin region to core region range from 4 to 10 μm versus 5 to 14 μm in HPDC AlCe44 alloy. While for the average volume fraction of eutectic, the HPDC AlLa44 alloy has value of 40.1% in skin region and 33.5% in the core, which corresponds to that of 36.5% and 21.4% in HPDC AlCe44 alloy, respectively. We conclude that HPDC AlLa44 alloy possesses finer microstructures and higher volume fraction of eutectic than HPDC AlCe44 alloy.

Microstructures of the interior regions of the two investigated alloys are presented in Fig. 2c and d clearly. These images were taken about 3 mm away from the skin

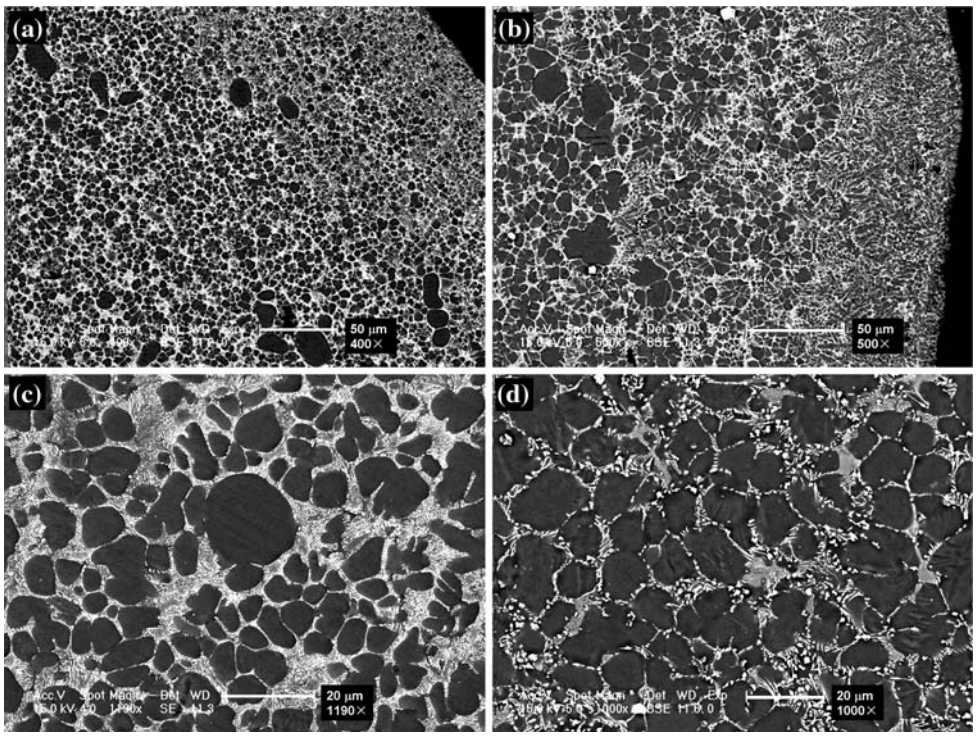

Fig. 2 Low-magnification images showing the skin and the interior regions: **a** HPDC AlLa44 alloy, **b** HPDC AlCe44 alloy; high-magnification images showing the interior regions: **c** HPDC AlLa44 alloy, **d** HPDC AlCe44 alloy

Table 2 Average grain size and volume fraction of eutectic of the two alloys in the skin and the core regions

Region	Average grain size (μm)		Average volume fraction of eutectic (%)	
	AlLa44	AlCe44	AlLa44	AlCe44
Skin	4	5	40.1	36.5
Core	10	14	33.5	21.4

surface. They reveal that both of the alloys are composed of primary grains of α-Mg solid solution (dark gray) surrounded by the high volume of eutectic (white). XRD patterns shown in Fig. 3 indicate that α-Mg solid solution and $Al_{11}La_3$ phase compose the HPDC AlLa44 alloy, while in the alloy of HPDC AlCe44 there exist α-Mg solid solution, $Al_{11}Ce_3$ and Al_2Ce phases.

Higher magnification inspection of the secondary phase at the grain boundaries in HPDC AlLa44 alloy, Fig. 4, reveals that the precipitates are not homogeneous in morphology. Two major types are distinguished. From Fig. 4a we could observe that acicular and lamellar precipitates congregate together and they are connected by crosswise branches. The acicular precipitates, approximately 3–8 μm in length (Fig. 4a) and 100 nm in diameter (Fig. 4c), are roughly parallel to each other. The distance between them has the same order of magnitude as their diameter. The lamellar precipitates are also roughly parallel to each other, and each slice grows like a dendrite (Fig. 4b). A correlation between the morphology and chemical compositions of

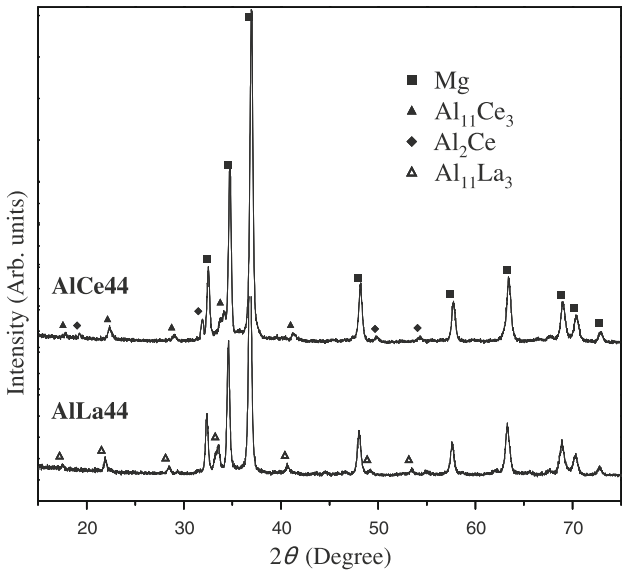

Fig. 3 X-ray diffraction patterns of the HPDC alloys

precipitates, which were identified by the SEM images, EDS analysis, and XRD results, reveals that both acicular and lamellar precipitates are $Al_{11}La_3$.

Higher magnification SEM analysis of the secondary phase morphology along the grain boundaries in HPDC AlCe44 alloy, Fig. 5, shows that three morphologies exist. In addition to the "rod-like and the congeries of acicular and lamellar" precipitates, polygonal precipitates are observed located along grain boundaries. The rod-like precipitates,

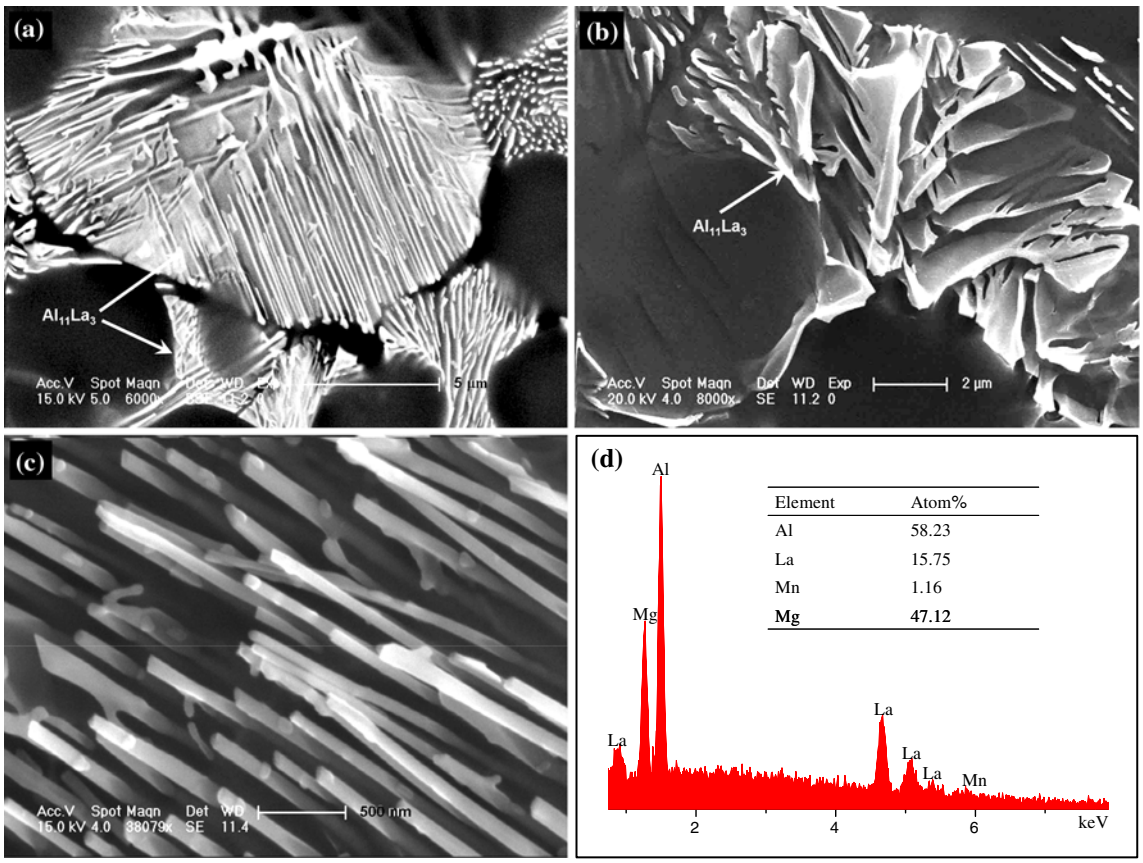

Fig. 4 SEM micrographs and EDS result of the secondary phase at grain boundaries of HPDC AlLa44 alloy

about several microns in length, are distributed relatively loosely at the grain boundaries. The acicular/lamellar compounds with diameter/width close to 100–200 nm and length up to several microns are arranged densely resulting in congeries and are mainly located at triple junctions. It should be noted that among the congeries the so-called "acicular" and "lamellar" precipitates grow together and it is not easy to distinguish between them. The minor polygonal precipitate phase, with sizes of about 0.3–1 µm, is distributed among the acicular and lamellar precipitates. The chemical formulas for the rod-like and acicular/lamellar precipitates are identified as $Al_{11}Ce_3$ and the polygonal precipitates are proved to be Al_2Ce phase by XRD and EDS results.

Mechanical properties

The effects of different RE (La vs. Ce) on the tensile properties of the HPDC AlLa44 and HPDC AlCe44, ultimate tensile strength (UTS), tensile yield strength (TYS), and elongation to failure (ε), from room temperature to 200 °C are listed in Table 3. The values of UTS, TYS, and ε at room temperature for AlLa44 alloy are 264 MPa, 146 MPa, and 13%, while for AlCe44 alloy are 250 MPa, 141 MPa, and 10%, respectively. At 200 °C, 118 MPa, 102 MPa, and 20% are the average values of UTS, TYS, and ε for AlLa44 alloy, which correspond well with those of 113 MPa, 98 MPa, and 17% for AlCe44 alloy. On the whole, both the AE alloys, AlLa44 and AlCe44, exhibit good mechanical performances including strength and ductility in the range of test temperatures. However, the mechanical properties of HPDC AlLa44 alloy are slightly better than those of HPDC AlCe44 alloy whether at room temperature or high temperatures. Figure 6 shows the SEM fractographs of tensile fracture surfaces of HPDC AlLa44 alloy tested at room temperature. From the SEM fractographs, large numbers of ductile dimples can be observed clearly. Significantly, almost all the $Al_{11}La_3$ precipitates are distributed around the dimples. This indicates that before fracture the tensile test bar has undergone certain plastic deformation and the fine $Al_{11}La_3$ particles are not the crack sources.

Creep properties

Typical tensile creep curves of HPDC AlLa44 and AlCe44 as well as the reference alloy AlCeLa44 containing Ce and La (our other research work, have applied for Chinese and American patent) carried out at 200 °C under a load of 70 MPa for 100 h are shown in Fig. 7a. The creep resistance

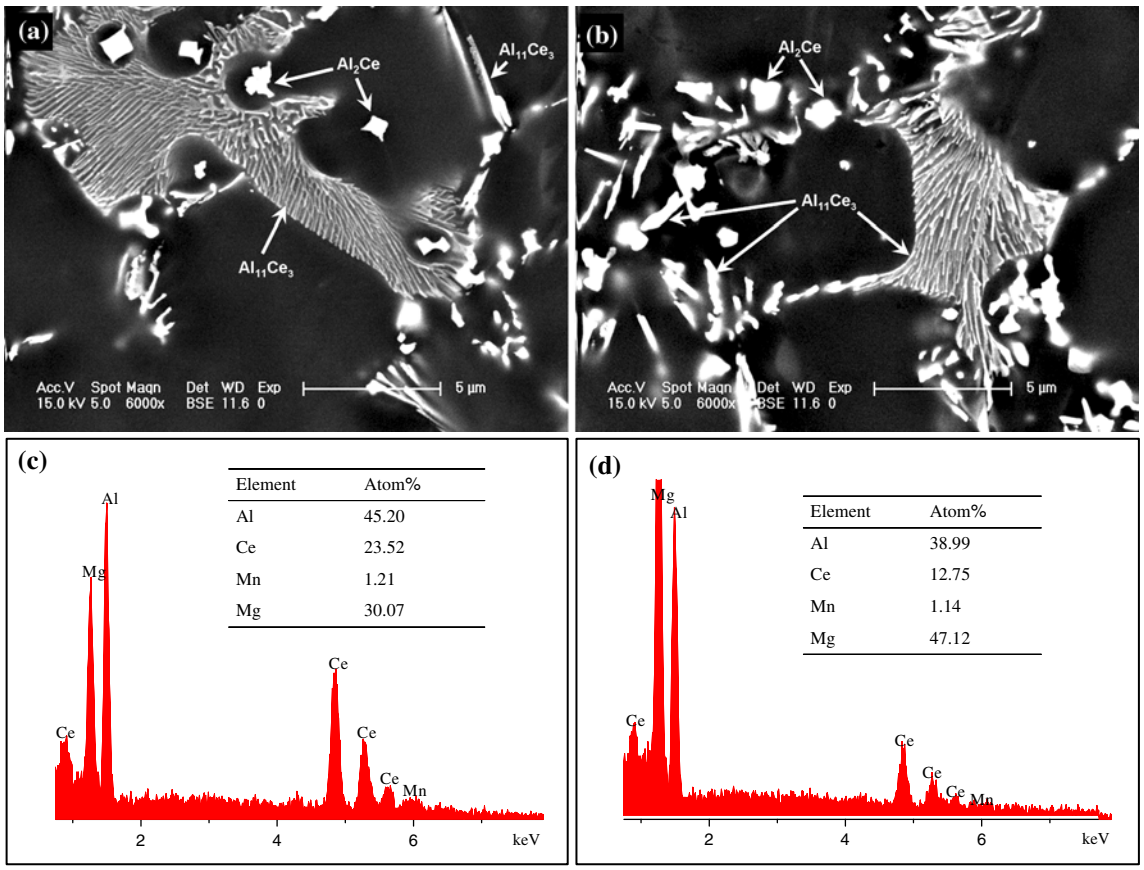

Fig. 5 SEM micrographs and EDS results of the secondary phases at grain boundaries of HPDC AlCe44 alloy

of HPDC AlLa44 alloy is better than that of HPDC AlCe44 alloy. As seen in Fig. 7b, the minimum creep rate of HPDC AlLa44 alloy obtained by measuring the slope of the creep curve at steady-state stage is 1.17×10^{-9} s^{-1}, while the value for HPDC AlCe44 alloy is $4.50 \times 10^{-9}s^{-1}$, about four times higher than that of HPDC AlLa44 alloy. The minimum creep rate of HPDC AlCeLa44 ranges between above two values. This implies that for strengthening the alloy against creep deformation the addition of lanthanum is more effective than that of cerium. The microstructures of the alloys before and after creep testing were characterized in detail.

As shown in Fig. 8a and b, after creep exposure no apparent morphology changes in microstructure are observed in HPDC AlLa44 alloy, which proves that the microstructure of HPDC AlLa44 alloy remains stable in the creep test. Nor can discernible changes be found in the XRD patterns of HPDC AlLa44 alloy before and after creep test (Fig. 9a). However, changes of morphology in near-grain boundaries are observed in HPDC AlCe44 alloy (Fig. 8c and d). It seems that the fine eutectic at the grain boundaries becomes incompact and coarse and the amounts of acicular or rod-like $Al_{11}Ce_3$ phase decrease in concomitance with the appearance of more polygonal Al_2Ce phase. Similar results have been reported for HPDC AE42 alloy that contains Ce-rich misch metal [9]. The corresponding XRD patterns of HPDC AlCe44 alloy before and after creep test are shown in Fig. 9b. They show a decrease in the relative intensity between $Al_{11}Ce_3$ and Al_2Ce phases. It appears that $Al_{11}Ce_3$ in the HPDC AlCe44 is unstable and has partly decomposed into Al_2Ce and free aluminum in the creep test. Consequently, the volume fraction of $Al_{11}Ce_3$ phase decreases possibly through phase transformations while that of Al_2Ce increases, at least under the creep test conditions of this study. However, no $Mg_{17}Al_{12}$ is found in this study as was reported for AE42 [9]. The reason for the absence of $Mg_{17}Al_{12}$ in our results may be that due to the higher content of rare earth elements (i.e., Ce) in AlCe44, most Al is present in the form of $Al_{11}Ce_3$ and Al_2Ce, with little Al sequestered as solute in the α-Mg matrix.

Discussion

High injection speeds, high metal pressures, and lack of efficient thermal barriers lead to extremely high cooling rates, which results in the refined microstructure. This is expected for HPDC alloys and is the common reason that HPDC AlLa44 and AlCe44 alloys demonstrated excellent

Table 3 Tensile properties of the HPDC AlLa44 and AlCe44 alloys at different temperatures (standard deviation is given in parenthesis)

Temperature (°C)	AlLa44			AlCe44		
	UTS (MPa)	YS (MPa)	ε (%)	UTS (MPa)	YS (MPa)	ε (%)
RT	264 (3.4)	146 (3.1)	13 (0.9)	248 (4.4)	140 (4.7)	10 (1.1)
120	182 (2.1)	128 (2.6)	23 (1.5)	172 (3.0)	126 (3.2)	22 (2.4)
150	148 (4.5)	112 (3.4)	27 (1.5)	140 (2.1)	109 (3.8)	27 (3.7)
175	135 (3.7)	108 (3.2)	25 (1.4)	123 (2.5)	103 (3.5)	21 (2.8)
200	118 (4.5)	102 (5.1)	20 (1.8)	113 (3.6)	98 (4.1)	17 (2.6)

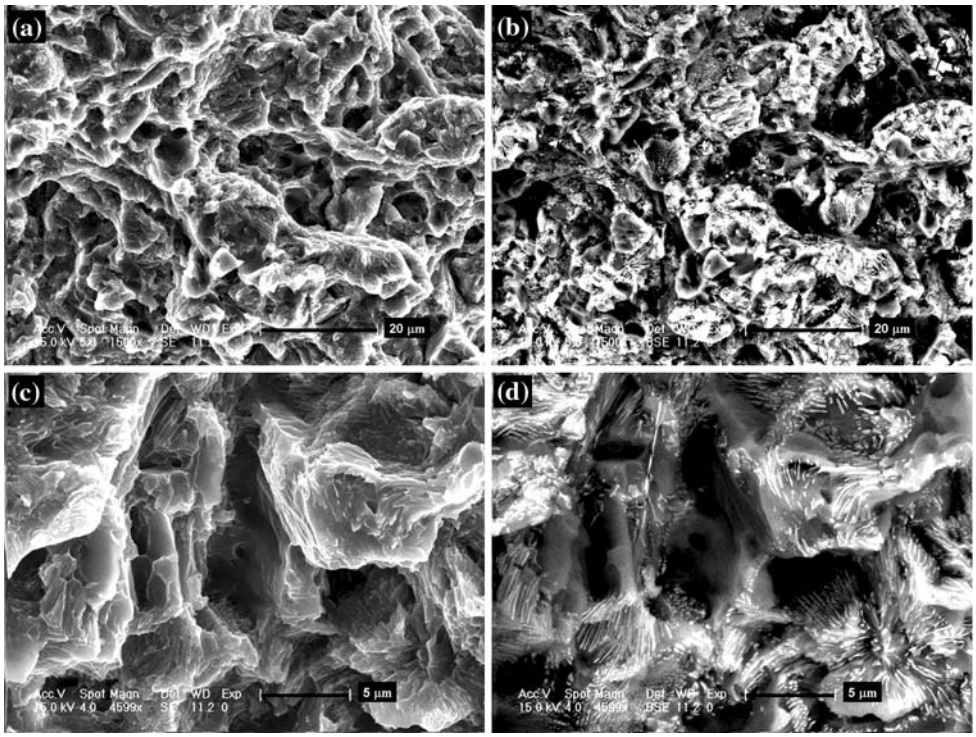

Fig. 6 SEM observation of the tensile fracture surface of HPDC AlLa44 alloy at room temperature: **a** and **c** secondary electron images; **b** and **d** backscattered electron images

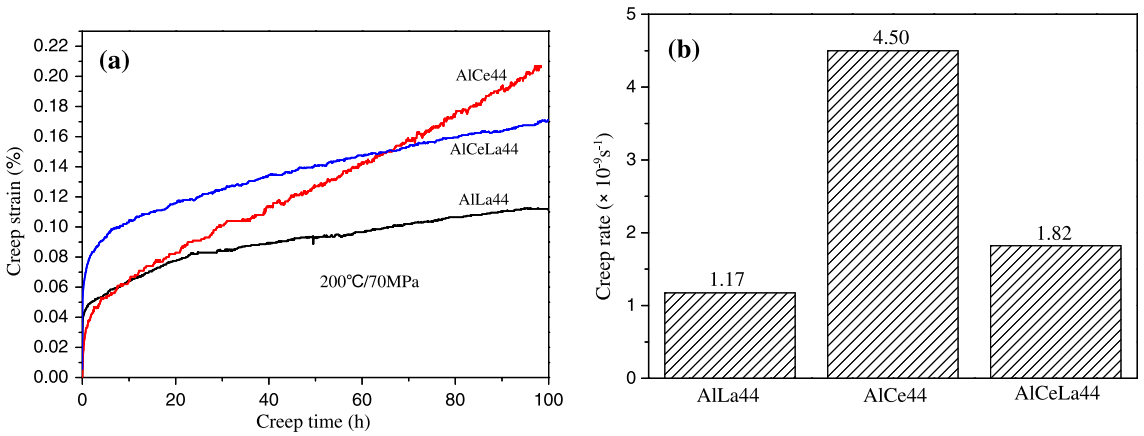

Fig. 7 Creep properties of the HPDC alloys, **a** creep curve and **b** steady state creep rate

mechanical properties. Therefore, the likely reason for the different microstructures and performances for the two HPDC alloys is that of the different rare earth elements.

The maximum solid solubility of La in Mg (0.79 wt%) is greater than that of Ce in Mg (0.16 wt%) [13], consequently more La atoms are utilized in the formation of

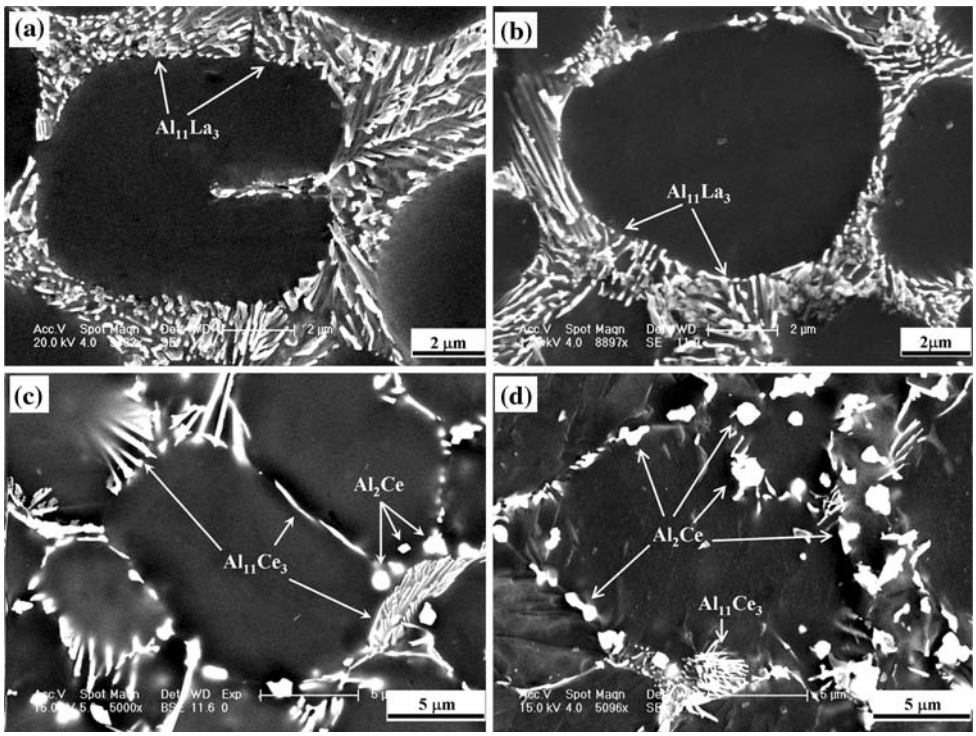

Fig. 8 SEM images of the HPDC alloys: AlLa44, **a** before and **b** after creep test; AlCe44, **c** before and **d** after creep test

intermetallic compounds. This is the main reason that HPDC AlLa44 alloy possesses higher volume fraction of eutectic than HPDC AlCe44 alloy. It has been reported that formation of either $Al_{11}RE_3$ or Al_2RE is sensitive to the individual rare earth element as evidenced by a relationship between the relative amounts of $Al_{11}RE_3$ versus Al_2RE and the La:Nd ratio (below about 0.7 Al_2RE was seen and above 0.7 $Al_{11}RE_3$ seemed to form) [9]. In the present work, only $Al_{11}La_3$ phase is formed in HPDC AlLa44 alloy, while besides the main secondary phase, $Al_{11}Ce_3$, small amounts of Al_2Ce phase are also observed in HPDC AlCe44 alloy.

Since HPDC Mg alloys are used in the as-cast condition, the relevant strengthening mechanisms of the two HPDC alloys are grain boundary/grain size effects as well as solid solution strengthening. The finer microstructure and higher volume fraction of secondary phases distributed along the grain boundaries provide better tensile properties for HPDC AlLa44 alloy. Of course, besides the volume fraction, other characteristics, such as size, morphology, and distribution of the secondary phases can also influence the mechanical properties of the alloy greatly. Compared with other alloying elements for creating heat-resistant magnesium alloys, e.g., Sr and Ca, La and Ce have a less harmful effect on ductility/fracture toughness [2]. For example, according to the literature [7], the elongation to failure of AJ43 (Mg–4Al–3Sr) and AJC421 (Mg–4Al–2Sr–1Ca) alloys is only 2.9% and 1.2% at room temperature, respectively. In the Ca- or Sr-containing alloys, which also have a high Al content [6–8, 14], many massive precipitations could be formed. Furthermore, they are the barriers which cannot be deformed and thus high stress concentration could be caused. Thus only a small degree of deformation would lead to internal crack opening. However, the outstanding microstructure of the two HPDC alloys, AlLa44 and AlCe44, is the "orderly stack" of the fine Al–RE intermetallic compounds (i.e., $Al_{11}La_3$ and $Al_{11}Ce_3$) formed at grain boundary regions, and this structure could provide considerable deformation when the high stress acts on the alloy. Based on the investigation carried out it can be concluded that the HPDC AE alloys, AlLa44 and AlCe44, have excellent combinations of strength and ductility.

Generally speaking, all the rare earth-containing phases could be effective for improving the creep resistance of magnesium alloys [15, 16], but the results of our creep tests reveal that the thermal stability increased in the following order: $Al_{11}Ce_3 < Al_{11}(Ce, La)_3 < Al_{11}La_3$, and the $Al_{11}La_3$ phase in HPDC AlLa44 alloy appears to be more effective for creep resistance than $Al_{11}Ce_3$ phase in HPDC AlCe44 alloy. On the other hand, we find that La:Ce ratio is higher in $Al_{11}(Ce, La)_3$ phase than that in $Al_2(Ce, La)$ phase in the reference alloy AlCeLa44-containing Ce and La. It suggests that compared with Ce, La more readily combines with Al to form $Al_{11}RE_3$ (RE = La) phase. As a consequence, it could infer that the stability of $Al_{11}La_3$ phase is higher than $Al_{11}Ce_3$ phase. At the same time, we turn to the theoretic calculation to elucidate the results of

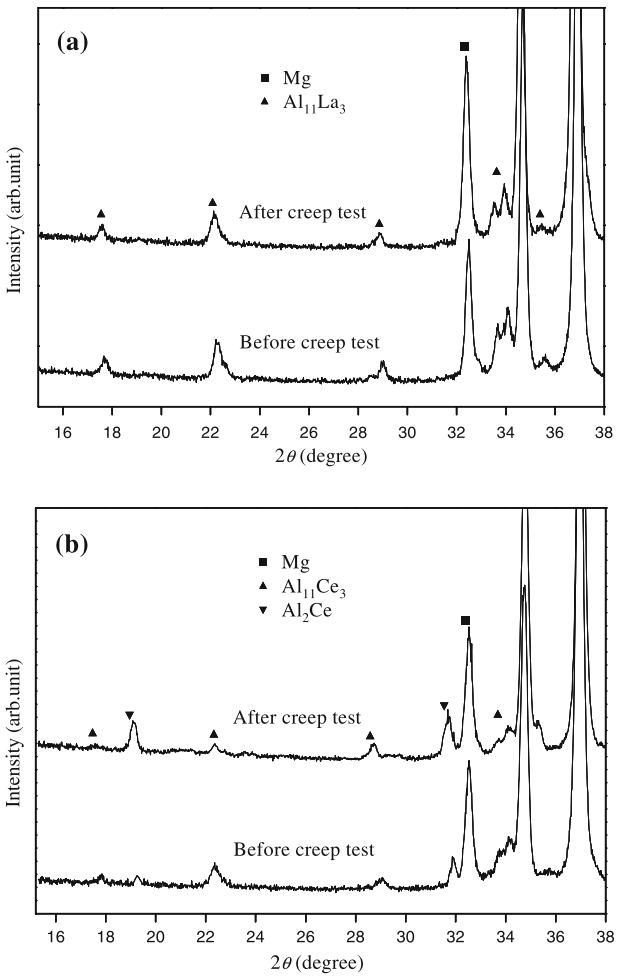

Fig. 9 XRD patterns of the HPDC alloys before and after creep test: **a** AlLa44, **b** AlCe44

our creep experiment. The calculations were performed by use of the CASTEP code [17] and Vanderbilt ultrasoft pseudopotential [18]. The exchange and correlation functions were treated by generalized gradient approximation in the formulation of Perdew, Burke, and Emzerhof (GGA-PBE) [19]. The self-consistent calculation was considered to be converged with the tolerance of 10^{-5} eV/atom. According to the reaction $Al_{11}RE_3 \rightarrow 3Al_2RE + 5Al$ [9], the decomposition energy ($\triangle E$) of $Al_{11}La_3$, $Al_{11}Ce_3$, $Al_{11}Pr_3$, and $Al_{11}Nd_3$ was calculated, respectively, and the results are shown in Table 4. It can be seen that among the four Al–RE intermetallic compounds the decomposition energy of $Al_{11}La_3$ is the highest. Considering these research results it is concluded that the thermal stability of $Al_{11}RE_3$ phase is sensitive to specific rare earth elements, and that $Al_{11}La_3$ phase in HPDC AlLa44 alloy is apparently more thermally stable than $Al_{11}Ce_3$ in AlCe44 alloy.

Owing to the $Al_{11}La_3$ phase existing in the grain boundary area, a very effective hindrance is provided to impede grain boundary sliding and dislocation motion in the vicinity of the grain boundaries. And also the general observations reported here indicate that the stability of microstructure, especially at the near-grain boundary regions, plays a crucial role in creep resistance for these fine-grained HPDC alloys [15].

Conclusions

Cored fine α-Mg grains surrounded by grain boundary regions which consist of eutectic phase, $Al_{11}La_3$, constitute the microstructure of high-pressure die-cast Mg–4Al–4La–0.4Mn alloy. While two binary Al–Ce phases, major $Al_{11}Ce_3$ and minor Al_2Ce, are formed at grain boundary regions in high-pressure die-cast Mg–4Al–4Ce–0.4Mn alloy. Better tensile properties are obtained in Mg–4Al–4La–0.4Mn alloy, in which the average values of UTS, TYS, and ε are 264 MPa, 146 MPa, and 13% at room temperature and 118 MPa, 102 MPa, and 20% at 200 °C, respectively. The excellent tensile properties are mainly attributed to the fine grains and grain boundaries containing fine secondary phases. The near-grain boundary microstructure of Mg–4Al–4La–0.4Mn alloy is apparently more stable during creep than that of Mg–4Al–4Ce–0.4Mn alloy, which is attributed to the better thermal stability of $Al_{11}La_3$ phase than that of $Al_{11}Ce3$ phase, and this provides a very effective hindrance to grain boundary sliding and dislocation motion in the vicinity of the grain boundaries during creep test. The results of this research provide a basis for further investigations of new high-pressure die-cast Mg–Al–RE alloys designed to serve at temperature of 200 °C.

Acknowledgements This project was supported by the Ministry of Science and Technology of China (2006AA03Z520, 2008DFR 50160), the Chinese Academy of Sciences, and Jilin Province. The authors also would like to thank Shanxi Wenxi Yinguang Magnesium Group for their assistance of preparation of samples.

Table 4 Decomposition energy of $Al_{11}RE_3$ (RE = La, Ce, Pr, Nd)

Kinds of RE	$E_{Al_{11}RE_3}$ (eV/atom)	E_{Al_2RE} (eV/atom)	E_{Al} (eV/atom)	$\triangle E$ (eV/atom)
La	−3235.5337	−982.2516	−57.1592	2.9828
Ce	−3835.0802	−1182.4250	−57.1592	2.0092
Pr	−4519.7980	−1410.3775	−57.1592	2.8695
Nd	−5307.0863	−1673.7845	−57.1592	−0.0632

References

1. Luo AA (2004) Int Mater Rev 49:13
2. Bakke P, Westengen H (2003) Adv Eng Mater 5:879
3. Pekguleryuz MO, Arslan Kaya A (2003) Adv Eng Mater 5:866
4. Pettersen G, Westengen H, Hoier R, Lohne O (1996) Mater Sci Eng A 207:115
5. Baril E, Labelle P, Pekguleryuz MO (2003) JOM 55:34
6. Zhao P, Wang Q, Zhai C, Zhu Y (2007) Mater Sci Eng A 444:318
7. Bai J, Sun Y, Xun S, Xue F, Zhu T (2006) Mater Sci Eng A 419:181
8. Bai J, Sun Y, Xun S, Xue F, Qiang J, Zhu T (2007) J Alloys Compd 437:247
9. Powell BR, Rezhets V, Balogh MP, Waldo RA (2002) JOM 54:34
10. Lee SG, Patel GR, Gokhale AM, Sreeranganathan A, Horstemeyer MF (2006) Mater Sci Eng A 427:255
11. Dahle AK, Sannes S, St John DH, Westengen H (2001) J Light Met 1:99
12. Lee SG, Gokhale AM (2006) Scr Mater 55:387
13. Zhang JH, Zhang DP, Tian Z, Wang J, Liu K, Lu HY, Tang DX, Meng J (2008) Mater Sci Eng A 489:113
14. Lü YZ, Wang QD, Ding WJ, Zeng XQ, Zhu YP (2000) Mater Lett 44:265
15. Moreno IP, Nany TK, Jones JW, Allison JE, Pollock TM (2003) Scr Mater 48:1029
16. Moreno IP, Nandy TK, Jones JW, Allison JE, Pollock TM (2001) Scr Mater 45:1423
17. Segall MD, Lindan PL, Probert MJ, Pickard CJ, Hasnip PJ, Clark SJ, Payne MC (2002) Phys Condensed Matter 14:2717
18. Vanderbilt D (1990) Phys Rev B 41:7892
19. Perdew JP, Burke S, Ernzerhof M (1996) Phys Rev Lett 77:3865